Superprism phenomenon in three-dimensional macroporous polymer photonic crystals

Tushar Prasad,[1] Vicki Colvin,[1] and Daniel Mittleman[2,*]
[1]*Department of Chemistry, MS-60, Rice University, 6100 Main Street, Houston, Texas 77005*
[2]*Department of Electrical and Computer Engineering, MS-366, Rice University, 6100 Main St., Houston, Texas 77005*
(Received 29 October 2002; published 11 April 2003)

The superprism phenomenon is the extremely large angular dispersion experienced by a light beam when entering a photonic crystal. This arises from the anisotropy of the photonic band structure. Strong anisotropy can be present even in systems without a complete photonic band gap. Here, we describe a theoretical investigation of the superprism effect in three-dimensional macroporous polymer photonic crystals formed from colloidal crystal templates. From the complete photonic band structure, an equal-energy surface (dispersion surface) is obtained. The propagation direction inside the photonic crystal is determined by the gradient of this surface. Using this formalism, we explore the extreme sensitivity of the propagation direction to various input parameters, including the input angle, the light frequency, and the composition of the photonic lattice. Such effects can be exploited for sensing and filtering applications.

DOI: 10.1103/PhysRevB.67.165103 PACS number(s): 42.70.Qs, 42.25.Bs, 07.07.Df

I. INTRODUCTION

Photonic crystals are periodic dielectric structures that control the propagation of light. In a photonic crystal, the refractive index is spatially modulated with a period comparable to that of the electromagnetic wavelength. As a result, constructive and destructive interference due to multiple scattering gives rise to a band structure for photons, which may contain gaps. These gaps may exist over the whole Brillouin zone or only within a limited range of wave vectors. Initially, the study of photonic crystals was motivated by the possibilities for inhibiting spontaneous emission[1] and localizing light.[2] Subsequently, most of the work in the field has relied on the control of light propagation through the manipulation of the gaps within the photonic density of states. As a result, the construction of a photonic crystal possessing a full band gap has been a primary goal of the field.[3] However, recently another method has been demonstrated for controlling the propagation of radiation inside a photonic crystal, involving the manipulation of the anisotropy of the bands.[4–6] Due to this anisotropy, the propagation direction of light inside a photonic crystal can be an extremely sensitive function of parameters such as the wavelength or the incident angle. This effect, known as the superprism phenomenon, is observed at high frequencies, where anisotropy in photonic band structure is strongest and effects like negative refraction and birefringence are expected.[7]

Various theoretical predictions and experimental studies have been reported regarding anomalous angular deviation at high frequencies near the photonic band gap. Lin *et al.*[8] reported beam deviation inside a two-dimensional (2D) crystal and attributed the deflection to non-linearity in the dispersion relation near the Brillouin zone edges. Subsequently, it has been realized that the anisotropy of the photonic bands plays a crucial role.[4,9] The propagation through photonic crystal prisms has been analyzed,[5,10] and a number of applications proposed.[6,11] This phenomenon has been studied using a transfer matrix approach, in both one and two dimensional crystals.[12,13] Other theoretical predictions involving the superprism effect have simulated auto-cloned 3D photonic crystals.[4,14,15] Very recently, Ochiai and Sánchez-Dehesa[16] have extended the discussion to the case of three-dimensional systems, such as self-assembled colloidal crystals.

In this work, we describe the computation of superprism effect in a macroporous polymer photonic crystal formed from a colloidal crystal template.[17] Following the method outlined by Kosaka *et al.* for two-dimensional photonic lattices,[5] we directly compute the isoenergy surface based on the full three-dimensional photonic band structure, and then determine the propagation angles from the gradient of this surface. Our simulations confirm a very sensitive dependence of the output angle on the parameters of the incoming beam. In particular, our calculations show a wavelength sensitivity of 14°/nm for an input wavelength of around 1300 nm, substantially larger than the 0.5°/nm dispersion recently reported for planar photonic crystals.[11] Calculations at constant wavelength show a change of 8° in the internal propagation angle for 1° change in the input angle. These sensitivities increase at lower wavelengths. The results substantiate the existence of superprism effect in three-dimensional photonic crystals, and emphasize the potential value of templated colloidal materials. Our technique is quite distinct from the method of Ref. 16, in which the analysis relies on the computation of a surface Brillouin zone rather than the complete dispersion surface. As a result, it is not readily generalizable to arbitrary crystal orientations. In addition to a plane wave expansion for calculation of the group velocity, this work also included an analysis of the coupling efficiency across the air-photonic crystal interface, based on a layer-Korringa-Kohn-Rostoker (KKR) method. This is required because the analysis is done for higher frequencies where many bands can couple. In contrast, we have not considered the issue of coupling, because at lower energies (such as considered here), it is not possible for more than a few bands to play a role. Finally, the technique described here only requires the numerical computation of the band struc-

ture, which can be performed to essentially arbitrary precision using available software.[18]

II. COMPLETE PHOTONIC BAND STRUCTURE

The basis for the superprism phenomena is anisotropy in the photonic band structure, a feature which is strongly present at frequencies near the photonic band gap. The effect is very sensitive to the particular choice of incident angle relative to the orientation of the photonic crystal, as well as the incident wavelength. Hence, accurate theoretical modeling is needed in order to design and orient samples for optimized sensitivity at a given wavelength. Here we apply our calculation to a particular crystal morphology, namely a macroporous polymer, which is robust and easy to fabricate.[19] These three-dimensional polymer photonic crystals are formed by using colloidal crystals as templates. Macroporous polymer templates can be prepared from high quality silica colloidal crystals with controlled thickness.[20] These are inverted face-centered-cubic (fcc) structures, i.e., interconnected air spheres in a close-packed fcc configuration in a polymer background.[19] Though these inverted structures do not provide a high enough dielectric contrast for the formation of a full band gap, they do possess substantial stop bands indicative of a partial gap along the {111} crystalline axis.[21] This is an indication of strong band structure anisotropy, which is sufficient for the manifestation of the superprism effect.

The band structure for the macroporous polymer is calculated using an available software package[18] which utilizes the plane wave method. This software computes definite-frequency eigenstates of Maxwell's equations in periodic dielectric structures for arbitrary wave vectors, using fully-vectorial and three-dimensional methods, and is specifically designed for the study of photonic crystals. For better convergence, a grid of $16\times16\times16$ is taken with mesh size of 7. To simulate the structure of macroporous polymer templates, we define the lattice geometry for the fcc lattice and set the ratio of sphere radius to the primitive unit cell length to be slightly more than 0.5, $r/a=0.53$. This corresponds to placing the air spheres slightly closer together than their diameters, leading to small windows which interconnect the internal air network.[22] This accurately reproduces the morphology of the samples.[19] The dielectric constant of the polymer background is taken as 2.5281 (corresponding to $n_p=1.59$), which is roughly the value for polystyrene.[23] The typical band structure for the lowest eight bands is shown in Fig. 1. Here, Ω is the normalized frequency given by $(\omega a/2\pi c)$ or (a/λ), where a is the length of the primitive unit cell.

The band structure shown in Fig. 1 is depicted in a standard way for the fcc lattice. It only displays the energy along lines connecting the high symmetry points on the Brillouin zone surface. However, a *complete* photonic band structure is needed to calculate the dispersion surface. In other words, we must calculate the band structure from the Γ point to *all* possible points on the Brillouin zone surface, not merely to the high symmetry points. We can of course use the symmetry of the Brillouin zone to reduce the computational load.

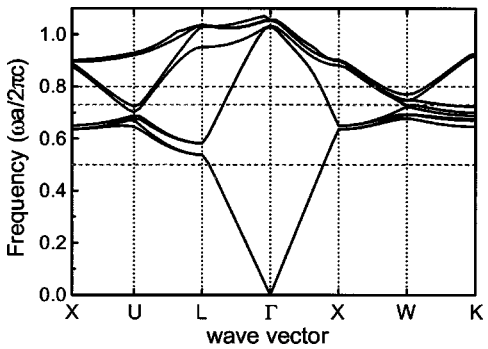

FIG. 1. The lowest eight bands in the band structure of the inverted fcc photonic crystal lattice, computed using the plane wave method (Ref. 18). The dielectric matrix has a refractive index of 1.59 (similar to polystyrene), and the air spheres overlap slightly $(r/a=0.53)$ in order to model an experimentally realizable sample. The horizontal dashed lines represent the energies used to compute the dispersion surfaces shown in Fig. 3.

III. DISPERSION SURFACE AND PROPAGATION DIRECTION

The complete photonic band structure gives information about how the band structure varies from Γ point to *all* possible points on the Brillouin zone surface. From this, all possible values of wave vectors in the three-dimensional space for a particular energy or frequency can be calculated. The plot of all these wave vectors in the **k**-space for a particular energy gives an equal-energy surface known as a dispersion surface. It is analogous to the index ellipsoid in conventional crystal optics or to the Fermi surface in electronic crystals.

The shape of the dispersion surface depends on the chosen value of energy, specified by the frequency of the incident light. For small values far below the stop band, the band structure is isotropic in nature. In this case the dispersion surface is spherical, with a radius given by the magnitude of wave vector which corresponds to a velocity of c/n_{ave}, where n_{ave} is the average (homogenized) refractive index. At high frequency values, near the photonic band gap, the band structure anisotropy is strong. As a result, the shape of dispersion surface deviates from spherical, though it retains the symmetry of the Brillouin zone.

To understand how this distortion of the dispersion surface leads to the superprism phenomenon, we first examine the band structure at small frequency values. Figure 2(a) shows the band structure for the second band at small frequency values, from the Γ point to five other high symmetry points on the Brillouin zone surface. At these values of frequency, the magnitude of wave vector for all five directions is nearly the same. As a result, the dispersion surfaces at these energies are spheres in k space. In contrast, Fig. 2(b) shows the band structure for the fourth band at higher frequencies. In this case there is a strong dependence of $|k|$ on the direction in k space. So at higher frequency values, a plot of the dispersion surface in **k**-space does not produce a sphere, but a distorted shape. The differences in the magnitudes of wave vectors in different directions for a particular

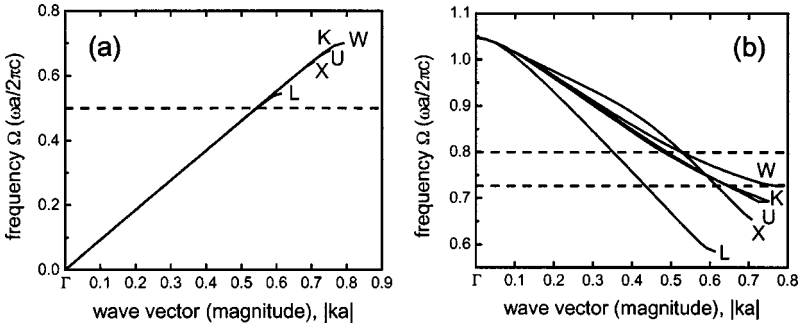

FIG. 2. Band structure from Γ point to five different high symmetry points on the Brillouin zone surface, plotted as the energy vs the magnitude of the dimensionless wave vector, $|ka|$. (a) shows the nearly isotropic second band, while (b) shows the anisotropic fourth band. The horizontal dashed lines represent the energies used to compute the dispersion surfaces shown in Fig. 3.

value of frequency are essentially the band structure anisotropy. In Fig. 3, examples of iso-energy surfaces are shown for the macroporous polymer sample under consideration, at the three energies denoted by horizontal dashed lines in Fig. 1. We note that these dispersion surfaces retain the symmetry of the Brillouin zone.

The propagation direction can be obtained directly from the dispersion surface.[4,5] First, the incident wave vector is obtained by drawing the free space dispersion surface (a sphere), and then drawing a ray from Γ point to a point on this surface to represent the incident wave vector $\mathbf{k}_{\mathrm{in}}$. The orientation of this incident wave vector defines the incident angles (θ_{in} and ϕ_{in}). The propagation wave vector inside the crystal is obtained by noting that the component of the wave vector parallel to the crystal surface is conserved across the boundary. Hence a corresponding point $\mathbf{k_P}$ on the photonic crystal dispersion surface is obtained, representing the propagation wave vector for the radiation inside the crystal. Finally, the propagation direction is obtained as normal to the dispersion surface at the end point of the propagation wave vector $\mathbf{k_P}$, since the group velocity v_g is given by $v_g = \nabla_k \omega(\mathbf{k})$. If the dispersion surface is spherical, then this gradient points radially, and the wave propagates in a direction parallel to its wave vector. As a result, the propagation angle does not change drastically for small changes in the incident orientation. However, if the dispersion surface is distorted, then the gradient can be a sensitive function of the incident angle. Sensitivity in wavelength arises from the fact that the shape of dispersion surface changes with small change in frequency. The more distorted the shape of the dispersion surface, the more drastic is the change in propagation direction and hence the more pronounced is the superprism effect.

We note that this analysis neglects the parity of the bands, which influences the coupling efficiency from free space into the photonic crystal modes, depending on the incident light polarization.[16] However, since in a three-dimensional lattice the modes are not pure TE or TM both *s*- and *p*-polarized lights exhibit some degree of coupling. We expect that *p*-polarized light couples more efficiently for the specific orientations described here because the modes have odd parity (with respect to the {110} symmetry plane in which the internal propagating *k*-vector is confined, as described below). In any event, the incident polarization is not relevant in computing the variation of the internal propagation angle with incident angle or wavelength, since the propagation direction is determined entirely by the shape of the dispersion surface.

IV. RESULTS AND DISCUSSION

With the computed dispersion surface, it is possible to calculate the incident and propagation angles with respect to any set of planes in the crystal, or equivalently for any arbitrary crystal orientation or facet. For illustrative purposes, we calculate here the results with respect to the {111} set of planes since they are most readily accessible experimentally.[19,20] We also report a few results for the {001} face since it is possible to grow the colloidal crystals with this face exposed by employing specially patterned surfaces.[24,25]

As we are dealing with three-dimensional crystals, the orientation of the incoming beam is defined by two parameters, θ_{in} and ϕ_{in}. Similarly, θ_p and ϕ_p define the internal propagation direction. The dispersion surfaces obtained at different frequencies differ in shape but retain the symmetry of the Brillouin zone. It is clear from Fig. 3 that the gradients of these dispersion surfaces will not, in general, point along a direction parallel to $\mathbf{k_P}$. However, due to the symmetry of the Brillouin zone, if $\mathbf{k}_{\mathrm{in}}$ lies in the plane $k_x = k_y$, then $\mathbf{k_P}$ will also lie in this plane, as will the propagation direction of the radiation. Hence, for this particular set of input wave vectors, the propagation direction can be parametrized by a single angle. This condition holds regardless of which crystal facet is exposed. We note that the dispersion surface offers

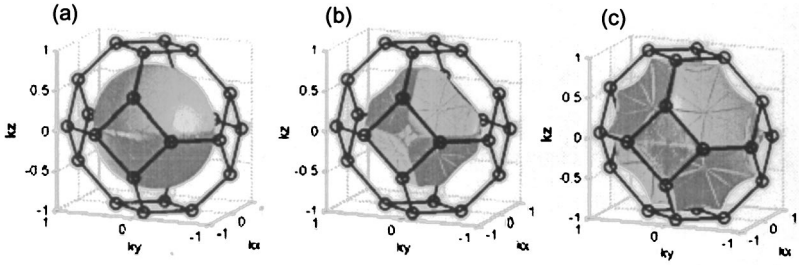

FIG. 3. Isoenergy (dispersion) surfaces computed from the full three-dimensional photonic band structure, a small portion of which is shown in Figs. 1 and 2. (a) Band No. 2, $\Omega = 0.50$. (b) Band No. 3, $\Omega = 0.80$. (c) Band No. 4, $\Omega = 0.73$.

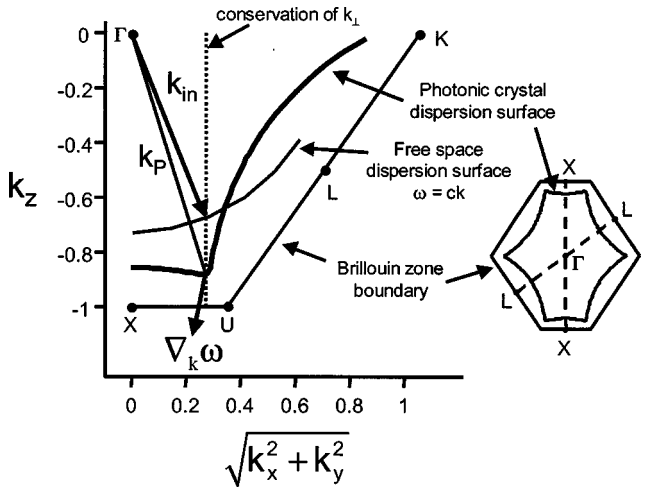

FIG. 4. One quadrant of a slice through the iso-energy surface shown in Fig. 3(c), along the plane $k_x = k_y$. The free-space and photonic crystal dispersion surfaces are shown, along with the edge of the Brillouin zone. This diagram illustrates the construction for determining the internal propagation direction for a given input ray. The vertical dashed line represents the momentum conservation condition for the component of **k** perpendicular to the surface normal (in this example, the {100} axis). The incident wave vector $\mathbf{k_{in}}$ (at an angle of 24° relative to the surface normal), the internal propagating wave vector $\mathbf{k}_P$, and the surface gradient (denoting the propagation direction) are shown. For this particular choice of input angle, the propagating ray exhibits negative refraction. The inset (at right) shows the full slice through the dispersion surface, along with the edge of the Brillouin zone.

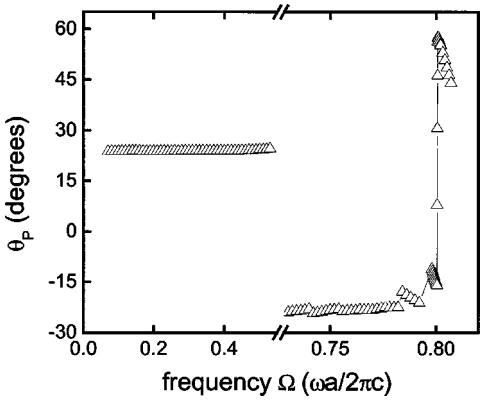

FIG. 5. Computed internal propagation direction as a function of frequency for an incoming beam incident on a {111} facet of the photonic crystal, at a fixed orientation of $(\theta_{in}, \phi_{in}) = (39°, 90°)$. Since $\phi_{in} = 90°$, the incident beam is in the $\{\bar{1}10\}$ plane, and as a result the propagating beam also lies in this plane.

an easy way to confirm this result, which otherwise requires a more complex analysis.[16,26–28]

Figure 4 shows one quadrant of a two-dimensional slice through the dispersion surface of Fig. 3(c), along the plane $k_x = k_y$. The inset shows the complete two-dimensional slice, along with the Brillouin zone boundary in this plane. This figure illustrates an example of the construction for determining the propagating wave vector. In this example, the incident energy is $\Omega = 0.73$ [as in Fig. 3(c)], and the incident angle is $\theta_{in} = 24°$ relative to the surface normal (which, in this case, is the {100} axis). The example shown here illustrates the phenomenon of negative refraction, which has been the topic of much recent discussion.[29–34] As noted previously, it is possible in a photonic crystal to have negative refraction without a negative effective refractive index.[35] This follows because the refraction is determined by the local anisotropy of the dispersion surface, as shown in Fig. 4. It should also be clear from this figure that a small change in the incident angle (in this case, a small increase) can move the resulting value of $\mathbf{k_P}$ across a region of substantial curvature on the dispersion surface, leading to a very large change in the propagation angle.

Figure 5 shows the variation of the internal propagation angle with frequency, this time for the case of a {111} input facet. As above, the input beam is confined in the $\{\bar{1}10\}$ plane, so the propagating beam is also confined in that plane and its direction is specified by a single angle. Here, we display the propagating angle θ_P for a fixed input orientation of $\theta_{in} = 39°$ relative to the {111} axis, as a function of the wavelength of the incident light. At small frequencies, θ_P is constant, with a value given by Snell's law as expected for an isotropic band structure. At high frequencies, $\theta_P < 0$, so negative refraction occurs. Near $\Omega = 0.80$, the propagation direction is a very sensitive function of frequency and there is a drastic change in the value of θ_P from negative to positive values. For an input wavelength of around 1300 nm, the angular dispersion in this region is of the order of 14°/nm. This is substantially larger than the values achieved in planar photonic crystals,[11] and could prove valuable for wavelength division multiplexing.

For beam steering applications, a relation between θ_P and θ_{in} for a particular value of frequency is needed. This result will of course depend on which crystal facet is exposed, due to the momentum conservation condition (see Fig. 4). However, as noted above, once the dispersion surface is determined it is easy to compute the result for any chosen crystal orientation. We discuss the two relevant cases mentioned earlier, for which the {100} and {111} faces are exposed. In both cases, the angles θ_P and θ_{in} are measured with respect to the surface normal. Figure 6 shows the computed relation between these two angles for (a) $\Omega = 0.30$ (band No. 2) and (b) $\Omega = 0.73$ (band No. 4), for the case of the {100} surface. The low frequency result is, unsurprisingly, smoothly varying and is consistent with Snell's law for the average (homogenized) refractive index. At the higher frequency, there is a sudden jump in the internal angle, from negative to positive values, at incident angles of roughly $\pm 25°$. The rate of change is approximately 8° for 1° change in the input angle. The variation of θ_P with θ_{in} is symmetric about $\theta_{in} = 0°$ (i.e., normal incidence), as a result of the fourfold symmetry of the dispersion surface. This symmetry can be seen in the inset to Fig. 4. In contrast, the {111} axis is not a symmetry axis for this dispersion surface, so the variation of θ_P with θ_{in} is not expected to be symmetric about the surface normal. Figure 7 shows the result for the case of the {111} surface; as in Fig. 6, the low frequency result ($\Omega = 0.30$) obeys Snell's law, while the result for a frequency higher in the band ($\Omega = 0.73$) ex-

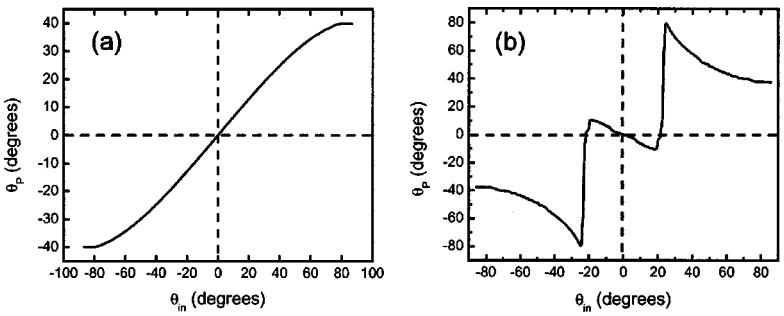

FIG. 6. Computed dependence of the internal propagation angle on the input angle. Both the input beam and the beam propagating inside the photonic crystal are confined in the $\{\bar{1}10\}$ plane. (a) $\Omega=0.30$. (b) $\Omega=0.73$. In both cases, the input facet is assumed to be a {100} lattice plane. The low frequency behavior (a) is consistent with Snell's law, whereas at high frequencies a strong angular dispersion is observed.

hibits discontinuities due to the warping of the dispersion surface. Also, we note in Fig. 7(b), for θ_{in} near 75° and −50°, there are two values of the propagation angle. This is a manifestation of the birefringence effect reported in earlier works.[5,16]

It is instructive to examine more closely the regions of high angular sensitivity, and explore the behavior for small variations in the input parameters. Figure 8 shows a close-up view of the sensitive region near 45° in Fig. 7(b), for several different closely spaced frequencies. It is clear from this plot that, in order to observe the superprism effect, both θ_{in} and the radiation frequency need to be carefully chosen. For example, for a frequency of $\Omega=0.8$, the extreme sensitivity to input angle occurs for an input angle θ_{in} of around 40°. A small shift in frequency, to $\Omega=0.82$, shifts the angle at which the effect occurs to about 37°. In this case, no significant effect is observed at input angles near 40°.

We can also explore the sensitivity to small changes in the refractive index of the macroporous polymer medium. As with small changes in the frequency, we expect that small variations in the properties of the photonic lattice can also lead to large changes in the internal propagation angle, within a certain narrow range of parameters. Small changes in the refractive index of the polymer backbone will lead to small variations in the curvature of the dispersion surface at a fixed frequency, which can shift the point at which the incident wave vector intersects this surface. Figure 9 shows a typical set of data illustrating this effect. Here we compute the internal angle θ_P as a function of the incident light frequency, for several different values of the polymer refractive index. As the index increases by steps of less than 0.1%, the frequency at which a large angular dispersion is observed shifts systematically to lower values. Calculations show that at around $\Omega=0.80$, a maximum change of around 70° in the propagation angle is obtained for 0.63% change in the polymer index.

This property can be applied to optical sensing. If the polymer which comprises the photonic crystal is also a recognizing agent for a certain analyte, then the presence of the analyte would lead to a small shift in the index of the photonic crystal, due to adsorption or chemical reaction with the polymer. This shift would in turn lead to a large change in the internal propagation angle, which may be more easily detected than the corresponding shift in the wavelength of the optical stop band.[36] We note that this sort of calculation is somewhat more cumbersome than for the earlier examples, since one must compute a new dispersion surface, not only for each energy, but also for each different refractive index. Nevertheless, the procedure, once the dispersion surface is determined, remains the same.

So far, all of our illustrative results have been restricted to the case where the *k*-vector of the input beam lies in the plane $k_x=k_y$, so that the internal propagating beam direction can be parameterized by a single angle. We have concentrated on this situation for ease of displaying the results. However, the superprism effect is still present even if this condition is not satisfied. As an illustration, Fig. 10 shows a portion of the three-dimensional dispersion surface for $\Omega=0.73$, along with the propagating ray and wave vector for a particular input ray. This illustrates the large out-of-plane propagation that can occur if the dispersion surface is warped. Figure 11 shows the calculated propagation direction for out-of-plane propagation, for a fixed orientation input ray at $(\theta_{\text{in}},\phi_{\text{in}})=(50°,85°)$, as a function of frequency. For small frequencies, the propagation beam stays in the plane of the incoming beam. But for high frequencies, both θ_p and ϕ_p are sensitive functions of frequency. There is large out-of-plane propagation and at around $\Omega=0.734$, both θ_p and ϕ_p change drastically. For frequencies above $\Omega=0.735$, ϕ_p reaches a constant value of around 93°. This behavior may offer improvement in previously described applications since beams of slightly different frequencies

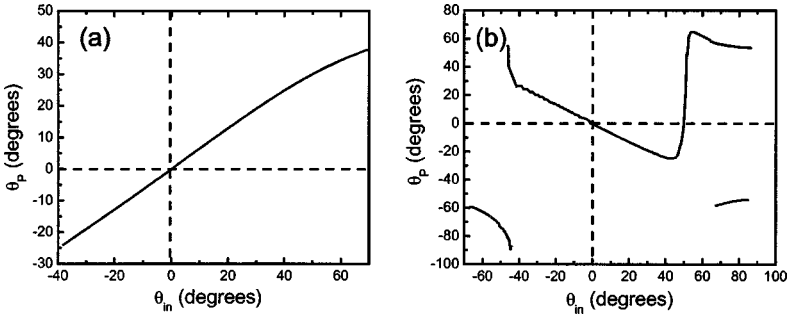

FIG. 7. As in Fig. 6, except that the input facet is a {111} lattice plane. Because the {111} axis is not a symmetry axis for the dispersion surface (see the inset to Fig. 4), the result in (b) does not exhibit symmetry about $\theta_{\text{in}}=0$. This result also shows multiple propagating solutions at high angles, consistent with earlier reports (Refs. 5 and 16).

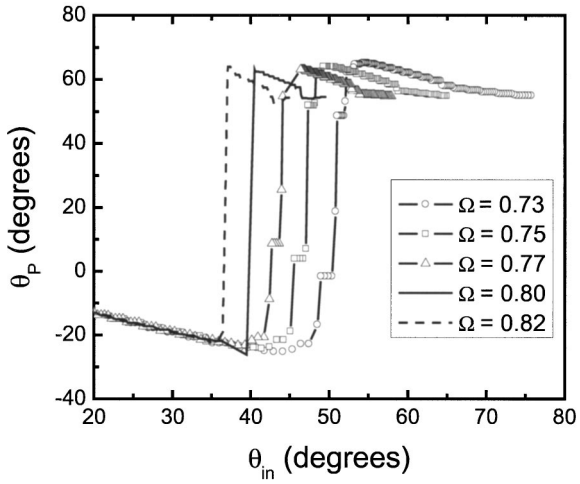

FIG. 8. A close-up view of the situation shown in Fig. 7(b), near the incident angle $\theta_{in}=45°$, for several closely spaced frequencies. The angle at which the superprism effect is observed is a sensitive function of the input frequency. However, the angular width of the transition region is not too sensitive.

would be much better resolved inside the photonic crystal. In order to observe such a large out-of-plane propagation as shown in Fig. 10, very thick crystals may be needed. The samples grown from colloids are typically only a few microns thick, although thicker high-quality crystals have been reported.[37]

Finally, as the calculated angle and wavelength sensitivities are very large, a consideration of experimental parameters is appropriate. An experimental realization of this effect depends on the degree of collimation of the incoming beam, an issue which has been considered recently by Baba *et al.*[38] We expect that, in order to clearly observe the extreme sensitivity of the propagation direction to the various parameters, it will be necessary for the input beam to be well collimated, so that the spread in incident angles is small compared to the angular width of the sensitive transition region. From a careful examination of Fig. 8, we note that the width of this transition decreases for increasing frequency Ω. However, even at a frequency of $\Omega=0.8$, the width of the transition is $\Delta\theta_{in}\sim 1°$ or ~ 17 mrad. An angular divergence of less than 1 mrad is readily obtained using many different laser sources. Even a focused beam does not exhibit too much divergence, as long as the focal length is not too small (e.g., $f>4$ mm for a 0.5 mm diameter input beam).

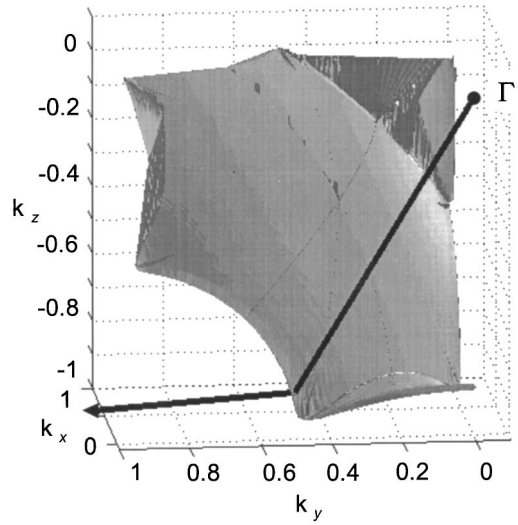

FIG. 10. An octant of the $\Omega=0.73$ dispersion surface (fourth band). Both θ_p and ϕ_p can change drastically if the incoming beam is not in the $\{1\bar{1}0\}$ plane. This is illustrated for an input ray with $\theta_{in}=137°$ and $\phi_{in}=89°$. Only the propagation wave vector (from the Γ point to the dispersion surface) and the propagation direction (arrow, $\theta_p=100°$, $\phi_p=37°$) are shown.

Another factor to consider is the influence of defects and disorder, which are inevitable in self-assembled structures. The role of uncontrolled defects in a photonic crystal is a matter of much current interest.[39] In the case of typical macroporous polymer photonic crystals, the presence of dis-

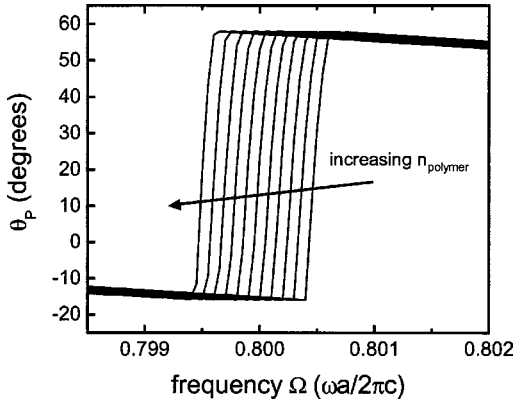

FIG. 9. Internal angle θ_P as a function of frequency, showing the sensitivity to small changes in the refractive index of the macroporous polymer backbone. In this calculation, the incident angle is fixed at $\theta_{in}=39°$ with respect to the {111} input facet. The eleven data curves show the result for polymer indices ranging from 1.59 to 1.60, in increments of 0.001.

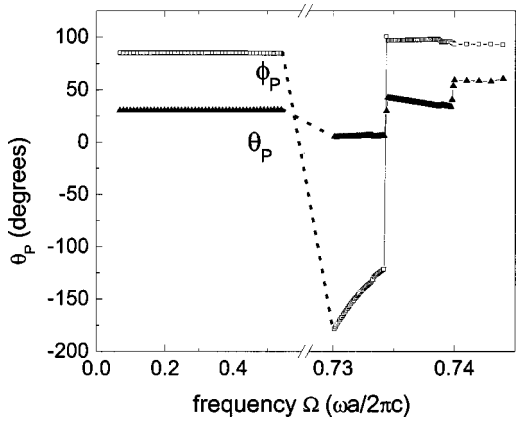

FIG. 11. Computed internal propagation direction as a function of frequency for an incoming beam incident on {111} face of the photonic crystal, at a fixed orientation of $(\theta_{in},\phi_{in})=(50°,85°)$. At high frequencies, the propagation beam is not confined in the plane of the incoming beam, and both θ_P and ϕ_P exhibit large angular dispersion.

order leads to scattering, which depletes the primary propagating mode and generates a diffuse background. This should have little impact on the measurements described here, unless the depletion of the primary mode is substantial. As long as there is sufficient energy left in the primary mode to determine its propagation direction, the superprism effect should still be observable. In fact, one could argue that the superprism geometry described in our work is one of the few proposed applications of these materials which is largely *insensitive* to disorder, since it relies only on a determination of the change in location (and not on an absolute measurement of the change in amplitude) of the transmitted beam.

V. CONCLUSION

We present an analysis of the superprism phenomena for a macroporous polymer photonic crystal, using a sample geometry that is readily fabricated. This method is an extension of the theory developed earlier for two-dimensional crystals, and is well suited to the study of the wide variety of complex morphologies that can be fabricated using templating techniques.[17,19] The superprism effect is observed in regions where the band structure anisotropy is substantial, although generally only for a narrow range of input parameters. This underscores the crucial role played by theoretical computation in the exploitation of this effect. Since the phenomena is only observable for a specific set of input orientations and laser wavelengths, a careful theoretical study is needed to properly design any experiment. The method presented here is quite flexible, in that it only requires the full band structure of the three-dimensional photonic lattice. We predict a very large angular dispersion of 14°/nm, more than sufficient for most wavelength division multiplexing applications. We also consider the possible applications of the superprism phenomenon to optical-based chemical sensing.

ACKNOWLEDGMENTS

This work was funded in part by the National Science Foundation and the Robert A. Welch Foundation.

*Corresponding author: Fax: (713) 348-5686. Email address: daniel@rice.edu

[1] E. Yablonovitch, Phys. Rev. Lett. **58**, 2059 (1987).
[2] S. John, Phys. Rev. Lett. **58**, 2486 (1987).
[3] A. Blanco *et al.*, Nature (London) **405**, 437 (2000).
[4] H. Kosaka *et al.*, Phys. Rev. B **58**, R10 096 (1998).
[5] H. Kosaka *et al.*, J. Lightwave Technol. **17**, 2032 (1999).
[6] H. Kosaka *et al.*, Appl. Phys. Lett. **74**, 1370 (1999).
[7] T. Baba and D. Ohsaki, Jpn. J. Appl. Phys. **40**, 5920 (2001).
[8] S. Lin *et al.*, Opt. Lett. **21**, 1771 (1996).
[9] M. Notomi, Phys. Rev. B **62**, 10 696 (2000).
[10] T. Baba and M. Nakamura, IEEE J. Quantum Electron. **38**, 909 (2002).
[11] L. Wu *et al.*, IEEE J. Quantum Electron. **38**, 915 (2002).
[12] B. Gralak, S. Enoch, and G. Tayeb, J. Opt. Soc. Am. A **17**, 1012 (2000).
[13] D. Felbacq, B. Guizal, and F. Zolla, J. Opt. A-Pure Appl. Opt. **2**, L30 (2000).
[14] T. Kawashima *et al.*, Appl. Phys. Lett. **77**, 2613 (2000).
[15] T. Sato *et al.*, Opt. Quantum Electron. **34**, 63 (2002).
[16] T. Ochiai and J. Sanchez-Dehesa, Phys. Rev. B **64**, 245113 (2001).
[17] P. Jiang, J. F. Bertone, and V. L. Colvin, Science **291**, 453 (2001).
[18] S. G. Johnson and J. D. Joannopoulos, http://ab-initio.mit.edu/mpb (1999).
[19] P. Jiang *et al.*, J. Am. Chem. Soc. **121**, 11 630 (1999).
[20] P. Jiang *et al.*, Chem. Mater. **11**, 2132 (1999).
[21] J. F. Bertone *et al.*, Phys. Rev. Lett. **83**, 300 (1999).
[22] R. Rengarajan *et al.*, Appl. Phys. Lett. **77**, 3517 (2000).
[23] E. S. Wilks, *Industrial Polymers Handbook* (Wiley-VCH, Weinheim, 2001).
[24] Y. Yin and Y. Xia, Adv. Mater. **14**, 605 (2002).
[25] S. M. Yang, H. Miguez, and G. A. Ozin, Adv. Funct. Mater. **12**, 425 (2002).
[26] N. Stefanou, V. Karathanos, and A. Modinos, J. Phys.: Condens. Matter **4**, 7389 (1992).
[27] N. Stefanou, V. Yannopapas, and A. Modinos, Comput. Phys. Commun. **132**, 189 (2000).
[28] F. Lopez-Tejeira *et al.*, Phys. Rev. B **65**, 195110 (2002).
[29] J. B. Pendry, Phys. Rev. Lett. **85**, 3966 (2000).
[30] M. C. K. Wiltshire, Science **292**, 60 (2001).
[31] R. A. Shelby, D. R. Smith, and S. Schultz, Science **292**, 77 (2001).
[32] Z. M. Zhang and C. J. Fu, Appl. Phys. Lett. **80**, 1097 (2002).
[33] M. W. McCall, A. Lakhtakia, and W. S. Weiglhofer, Eur. J. Phys. **23**, 353 (2002).
[34] N. Garcia and M. Nieto-Vesperinas, Opt. Lett. **27**, 885 (2002).
[35] C. Luo, S. G. Johnson, and J. D. Joannopoulos, Phys. Rev. B **65**, 201104 (2002).
[36] J. H. Holtz and S. A. Asher, Nature (London) **389**, 829 (1997).
[37] Y. A. Vlasov *et al.*, Phys. Rev. E **61**, 5784 (2000).
[38] T. Baba and T. Matsumoto, Appl. Phys. Lett. **81**, 2325 (2002).
[39] J. F. Galisteo Lòpez and W. Vos, Phys. Rev. E **66**, 036616 (2002).